The Role of LiDAR Data in Understanding the Relation Between Forest Structure and SAR Imagery

Richard Lucas[1], Alex Lee[2] and Mark Williams[3]
[1]*Institute of Geography and Earth Sciences, the University of Wales, Aberystwyth, Ceredigion, SY23 3DB, United Kingdom (phone: +44 1970 622612; fax: +44 1970 622659; e-mail: rml@aber.ac.uk).*
[2]*SRES, Australian National University, Canberra, ACT, Australia (email: Alex.Lee@anu.edu.au)*
[3]*IMES Group, Defence Science and Technology Office (DSTO), PO Box 1500, Edinburgh, SA5111, Australia (email: Mark.Williams@defence.dsto.gov.au)*

Abstract— **As part of the 2000 PACRIM II Mission to Australia, polarimetric Synthetic Aperture Radar (SAR) data were acquired near Injune, central Queensland, Australia. The primary purpose of the acquisition was to better understand the role of SAR for retrieving biophysical properties of native forests through either empirical relationships or simulation modeling. In this paper, we outline the generation of a three-dimensional representation of the forest structure and component elements (leaves, branches and trunks) using field, airborne LiDAR and CASI data and aerial photography acquired at the same time as the AIRSAR. We then show how this representation formed the basis of the input to a coherent SAR imaging simulation that models microwave penetration and interaction with canopy and understorey components. A preliminary comparison between actual AIRSAR and simulated SAR data for a poplar box (*Eucalyptus populnea*) woodland suggests effective modelling of SAR backscatter.**

***Index Terms*—Forestry, radar, scattering, simulation.**

I. Introduction

In understanding microwave interaction with different components of forests, a number of approaches have been used including the use of empirical relationships and modeling using two-dimensional layers or cubes [e.g., 1,2]. In the latter case, the cubes or "voxels" have typically been constructed around artificial trees or those that have been measured from field data.

In this study, we demonstrate the use of airborne LiDAR data for constructing a three-dimensional voxel grid of selected forest sites in Queensland, Australia. We use a crown delineation algorithm on the LiDAR data to associate voxel groups with tree crowns or clusters. These crowns/clusters are then classified by species using hyperspectral Compact Airborne Spectrographic Imager (CASI) and Large Scale (1:4000) Aerial Photography of the same forests. For each crown/cluster, we attribute associated voxels with species-specific parameters relating to the biomass and structure of the forest. In a separate process, we reconstruct the dimensions and orientations of primary, secondary and tertiary branches from the LiDAR point data. The ground surface is also characterized using field observations and classifications undertaken through spectral unmixing of CASI data. Using this information, we parameterize a coherent SAR image simulation model that considers microwave penetration and interaction with canopy and understorey components. Outputs from the simulation at L-band are illustrated and compared against the actual AIRSAR data.

II. Site Description

The study focused on an area of mixed species forests near Injune in central Queensland, Australia (Latitude -25° 32', Longitude 147° 32'). A full description of the study area is given in [3]. In preparation for the acquisition of aerial photography, airborne LiDAR and hyperspectral data as well as Synthetic Aperture Radar (SAR), a grid of 150 500 x 150 m Primary Sampling Units (PSUs) was established, with each separated in the north-south and east-west directions by approximately 4 km. PSUs were numbered sequentially from top left (1) to bottom right (150), with each containing 30 Secondary Sampling Units (SSUs) numbered sequentially from 1 to 30. For this particular study, a 150 x 500 m section (PSU 142) of Poplar Box (*E. populnea*) forest was considered. Further analyses were also undertaken for other forests but these are reported in a separate paper. This forest contained relatively sparse cover with a biomass ranging from 43 Mg ha^{-1} to 80 Mg ha^{-1} for the contained SSUs. Although *E. populnea* dominated, individuals of other species, including Brigalow (*Acacia harpophylla*), White Cypress Pine (*Callitris glaucophylla*) and Silver-leaved Ironbark (*E. melanaphloia*) were also present, although each represented no more than 5 % of the trees present. In sections, a 5-6 m high understorey consisting of Sandalwood Box (*Eremophila mitchelli*) occurred. The forests ranged from thinned (typically ring-barked) stands, which contained a significant proportion of regenerating individuals, to "old-growth" trees. In both cases, significant grazing by stock had occurred.

0-7803-9051-2/05/$20.00 (C) 2005 IEEE

III. DATA COLLECTION

A. Acquisition of LiDAR and hyperspectral data

For the 37 x 60 km study area, LSP were acquired in July, a month before the main field campaign in August, 2000. Airborne scanning LiDAR data were acquired subsequently over a one-week period commencing August 24th, 2000, using an Optech 1020 scanning LiDAR mounted in a Bell Jet Ranger Helicopter. The Optech measured 5000 first and last returns and the intensity of each return per second. The LiDAR operated within the NIR spectrum with a beam divergence of 0.3 milliradians, a footprint of approximately 7.5 cm and an average sampling interval of < 1 m. Data were acquired flying in an east-west direction (and centred on each PSU row) at a nominal altitude of 250 m and a swathe width of approximately 200 m. A GPS base station was established for all flights. With full differential GPS corrections in addition to pitch, yaw and roll compensation from an Inertial Navigation System, coordinates were provided with an absolute accuracy of < 1 m in the x and y directions and < 0.15 m in the z direction.

Over a similar time-period, 1 m spatial resolution Compact Airborne Spectrographic Imager (CASI) data were acquired over the same areas as the LiDAR, although the aircraft flew in a north-south direction. Full calibration of the CASI data was achieved by laying out pseudo-invariant features (PIFs) at the time of the CASI overpass and collecting reflectance measurements from these using an ASD field spectroradiometer. Empirical line techniques were used. Several north-south Hyperspectral HyMap images (~ 1.2 m swath width) were also acquired in September, 2000 and consisted of 128 bands of data at 2.6 m spatial resolution.

B. Forest inventory and destructive harvesting

At the same time as the LiDAR and CASI data were acquired, forest inventory data were collected from selected SSUs located within 12 of the 150 PSUs [3]. These data consisted of basic forest inventory measurements for each tree including diameter at 30 and 130 cm (D30 and D130 respectively), the heights to the top, canopy base and first leafing branch and crown dimensions in the east-west and north-south dimensions. Each tree measured was identified to species and most (including all those in PSU 142) were photographed using a digital camera. The growth stage of individual trees was also recorded. Soil measurements were taken for different forest types (e.g., clay, sand) and included gravimentric moisture content, bulk density and dielectric constant (using a TDR). Leaf size (length, width and thickness) was also measured in the field and laboratory.

Following the collection of field data, destructive harvesting of *C. glaucophylla* (n = 22), *E. populnea* (n = 7) and *E. melanaphloia* (n=5) was undertaken to derive new allometric equations for estimating the biomass of *C. glaucophylla* but also to obtain biomass estimates for assessing the validity of using existing equations for *E. populnea* and *E. melanaphloia*. Harvesting was undertaken such that allometric equations relating tree size (D30, D130, height and crown area) to the biomass of the leaves, branches (< 1 cm, 1-4 cm, 4-10 cm and > 10 cm) and trunk. Estimates of gravimetric moisture content were also obtained for these components.

IV. MODEL PARAMETERISATION

A. Trunk location and tree crown/cluster delineation

The identification of tree trunks was achieved using a height-weighted crown openness index (HVCOI), which equates to the relative penetration of the LiDAR beam through the forest volume (Fig. 1). A high openness indicates a greater likelihood of penetration to the ground surface as relatively few leaves and branches are there to intercept the LiDAR pulse. To locate low points, the Arc Topogrid function was used to create a 'hydrologically' corrected interpolated openness surface of 1 m^2 cell size and a corresponding 'sinks' layer used to identify local points within the openness images. Comparison of these 'sink' points with actual tree locations suggested a close correspondence, with omissions associated with trees which are either senescent, small or beneath the canopy of larger overstorey trees.

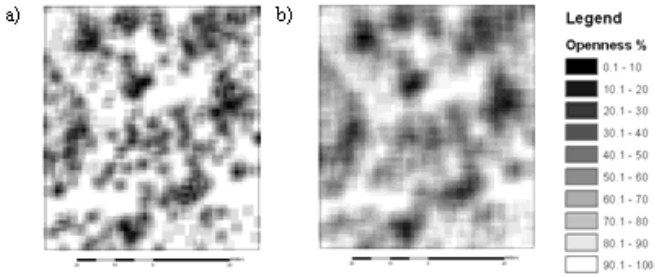

Fig. 1. Openness surface generated from LiDAR data and smoothed using a) a 3 x 3 and b) a 5 x 5 window surface. Darker areas correspond to tree trunk locations.

Tree crowns or clusters were delineated subsequently by intersecting the original point coverage with the openness grid and iteratively contouring the resulting openness values linked to the threshold where 90 % of the original LiDAR returns > 2 m in height had been captured. Depending upon the structure of the forests, the openness contour providing the optimal delineations varied from 75 to 90 %.

B. Tree species discrimination

The discrimination of tree species was undertaken primarily using CASI data but also with reference to Large Scale (1:4000) aerial photography because of some cloud shadow in the scene. For PSU 142, discrimination was based largely on spectral differences between crowns and each delineated crown/cluster was manually associated with species. The differentiation of species was assisted using a delineation process developed using eCognition software. Each delineated crown or cluster was then associated with information on species and height, as determined from the CASI/LSP and LiDAR data respectively. On this basis,

crowns could then be associated with an estimate of leaf, branch (< 1 cm, 1-4 cm, 4-10 cm and > 10 cm) and trunk biomass through application of species-specific allometric equations. As the weights of the leaves of different species was known and those of small branches could be approximated from volume measurements (based on known measurements of start and end radius of branches and length), the number of leaves and small branches per tree could also be estimated.

The ground surface was also classified using the CASI data into classes of bare soil, non-photosynthetic vegetation (NPV; namely dry grass) and low shrubs using supervised classification techniques. Standing or fallen dead wood was also mapped using the CASI data and with reference to field surveys of the location and dimensions of material. A 1 m spatial resolution digital elevation model derived from the LiDAR data was integrated into the surface classification.

C. Voxel construction and parameterisation

The construction of LiDAR voxels was initiated by forming a 1 m^2 fishnet to cover the maximum geographical extent of the LiDAR data and creating 1 m height intervals from the ground surface to the tallest height recorded. This created "virtual" voxels, where a voxel (in this case, 1 m^3) is defined using the combination of cell (*x, y*) and height intervals (*z*) over the plot volume. The LiDAR point layer was then intersected with the voxel matrix layer such that the height above ground was recorded for the corresponding voxel in the matrix. Where multiple returns occurred within one voxel, the maximum height and the number of returns were recorded.

Within this matrix, voxels were then associated with crowns/clusters delineated using the openness surface through geographical reference. Then, for each tree, voxels were collectively attributed with information on species and height as well as basic structural attributes (e.g., leaf length, radius, thickness and gravimetric moisture content). The number of leaves and small (< 1 cm diameter) branches within each voxel was estimated by dividing the total number for the tree by the number of associated voxels.

D. Primary and secondary branches

The distribution of primary and secondary branches was approximated from the LiDAR data. For each tree, the primary branches were associated with voxel clusters identified using criteria based on relative height, polar angle and adjacency. Typically, up to seven clusters per tree were found, although this varied with height and crown dimensions. The locations of the primary branch end points were associated with the voxel centroids. The location of the primary branch start point (i.e., the join with the trunk) was then determined using species-specific zenith angle distributions established using digital photographs of field trees and angular geometry. In some cases, the estimated join point was too close to the base of the tree and the location was therefore associated with the height of the first leafing branch. This position was estimated using species-specific relationships between field measurements of height to the tree top and the first leafing branch. Secondary branches were then constructed from the base of the voxels associated with each primary branch to positions along the primary branch. These latter positions were based on proportional distance of each voxel base to the origin of the primary branch. Adjustments to secondary branch origins were necessary to compensate for voxels that were initially grouped with a primary branch cluster but were then considered to be too far away or at an unrealistic angle from the primary branch. The model input consisted of the primary and secondary branch start and end position in *x*, *y* and *z* coordinates, radius (based on tree diameter and radius/length functions) and also polar angle. Small tertiary branches (< 1 cm) were confined to the voxel space and were allocated a length of 0.5 - 1 m and a direction compatible with the polar and zenith angle distributions of the secondary branches to which they joined.

E. SAR simulation

The ground surface classifications, voxel-parameterised file and both the trunk and branch maps were combined to provide a full 3D reconstruction of the forest and ground. The information content was such as to permit description of the forest for the purpose of radar calculations. These were performed using a unique, coherent SAR imaging calculation developed at DSTO, Australia. Specifically, model calculations were performed using a mean field model, but one in which canopy spatial inhomogemeity was properly accounted for. A unique feature of the simulation is that it produces synthesized, fully coherent and polarimetric, single-look-complex SAR imagery. Images calculated using the technique may also be analyzed as real observations. A full description of the methods used may be found in [4]. For the purposes of this paper, calculations at L-band were performed (at 5 m spatial resolution) using the same platform motion and center frequency as the AIRSAR. Comparison between simulated and AIRSAR imagery for PSU 142 was also undertaken.

V. RESULTS

A. Tree and stand reconstruction

A graphical representation of a section of the reconstructed stand at PSU 142 is given in Fig. 2 and compares favorably with the photographs of the area.

Fig 2. Graphical output from DSTO radar simulation of part of the reconstructed canopy at Injune PSU site 142.

B. L-band coherent simulations

The simulation of the SAR backscatter at L-band HH, VV and HV for individual trees and for PSU 142 is shown in Fig. 3

and may be compared with the AIRSAR image in Fig 4. We note that there is loss of dynamic range in the AIRSAR image as a result of data compression techniques, and that the simulated image is Single Look Complex, 5 m resolution, whilst the AIRSAR is multi-looked, which further serves to reduce variance in intensity. The pixel spacing in both cases is 2.6m and the simulated area is 150m by 500m corresponding to the central area of the larger AIRSAR image, which is 230m by 606m. Fig. 3 shows that there is a clear delineation between densely forested and sparsely populated areas in the simulated SAR imagery. HH is brighter than VV, and HV seems to be underestimated in the first order model.

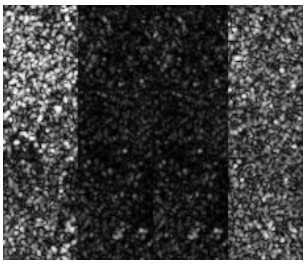

HH HV VH VV

Fig. 3. Simulations of L-band imagery from individual *E. populnea* trees and for PSU 142.

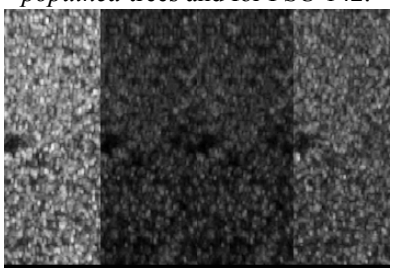

HH HV VH VV

Fig 4. AIRSAR image of area including PSU142.

C. Comparison between actual and simulated SAR data

To determine how well the L-band backscatter was simulated by the model, comparisons with actual AIRSAR data were undertaken for PSU 142. Registration of the AIRSAR data was achieved by establishing common Ground Control Points (GCPs) between individual trees identified within the HyMap data (registered using GPS and INS) and P-band HH data, as the phase centre is close to the base of the trunks. Backscattering coefficients were derived from the simulated imagery and compared with those recovered from the AIRSAR image (Table I).

TABLE I. Backscattering Coefficients. Note that DG, DV and GV represent direct ground scattering, direct volume and ground volume scattering respectively.

	HH	HV	VV
DG	-27.9	-52.8	-21.9
DV	-19.8	-26.9	-17.9
GV	-13.7	-38.1	-24.4
Total (Sim)	-12.6	-26.6	-15.8
Total (JPL)	-12.7	-22.5	-17.4

Comparison with AIRSAR is very favorable with total response differing mostly in HV, which is anticipated to be underestimated in a first order model of this kind. As with previous models, a breakdown of total return by scattering mechanism is possible and shows that in HH, ground volume (GV) returns are the most important whereas in HV and in VV, direct volume returns predominate. This is in agreement with the results of [3].

VI. CONCLUSIONS

The study is unique in that it is the first to integrate field data (including destructive harvesting measurements), LiDAR and CASI/LSP to reconstruct a forest stand and to provide attributes relating to ground surface properties and the size (volume), orientation and dielectric properties of vegetation elements. The resulting SAR simulations provide a realistic overview of backscatter at L-band and the approach provides good insight into the potential of data from existing or forthcoming sensors (e.g., the ALOS PALSAR) for retrieving forest structural attributes.

ACKNOWLEDGMENT

The authors thank the Defence, Science and Technology Office (DSTO), the Queensland Department of Natural Resources and Mines (QDNR&M), Bureau of Rural Sciences (BRS), Australian Greenhouse Office and CRC for Carbon Accounting and the Queensland Department of Primary Industries (QDPI) Tropical Beef Centre for assisting with destructive harvesting.

REFERENCES

[1] M.C. Dobson, F.T. Ulaby, T. LeToan, A. Beaudoin, E.S. Kasischke and N. Christensen, "Dependence of radar backscatter on coniferous forest biomass," IEEE Trans. Geosci. Remote Sensing, vol. 30(2), pp. 412-415 , 1992.

[2] Sun, G., Ranson, K.J., and Kharuk, V.I., 2002. Radiometric slope correction for forest biomass estimation from SAR data in the Western Sayani Mountains, Siberia. *Remote Sensing of Environment*, 79(2-3), pp. 279-287.

[3] Lucas, R.M., Moghaddam, M. and Cronin, N (2004). Microwave scattering from mixed species woodlands, central Queensland, Australia. IEEE Transactions on Geoscience and Remote Sensing, 2142-2159, October, 2004

[4] S R Cloude, D G Corr and M L Williams, "Target Detection beneath Foliage using Polarimetric Synthetic Aperture Radar Interferometry", *Waves in Random Media* 14 (2004) p. S393-S414.